In-silico analysis of device-related thrombosis for different left atrial appendage occluder settings

Eric Planas[1], Jordi Mill[1], Andy L. Olivares[1], Xabier Morales[1], Maria Isabel Pons[1], Xavier Iriart[2], Hubert Cochet[2], and Oscar Camara[1]

[1] PhySense, Department of Information and Communication Technologies, Universitat Pompeu Fabra, Barcelona, Spain
[2] Hôpital de Haut-Lévêque, Bordeaux, France

Abstract. Atrial fibrillation (AF) is one of the most common cardiac arrhythmias and is associated to an increasing risk of stroke. Most AF-related strokes are formed in the left atrial appendage (LAA). To prevent thrombus formation, LAA occlusion (LAAO) is considered a suitable alternative for AF patients with contraindications for anti-coagulation treatment. Nevertheless, LAAO is linked to a non-negligible risk of generating thrombus at the surface near the device (i.e., device-related thrombus, DRT), depending on the implantation settings. For instance, it has been shown that not covering the pulmonary ridge (PR) with the LAAO increases the risk of DRT. In-silico analysis is a useful tool to better understand the blood flow patterns after LAAO and predict the risk of DRT for a given patient and device configuration. In the present work we designed a modelling pipeline based on fluid simulations, including a thrombus model using discrete phase modelling, to analyse the risk of DRT in six patient-specific geometries for different LAAO settings. In particular, we studied the possible incidence of DRT depending on the device positioning (covering/uncovering the PR) and type (Amplatzer Amulet and Watchman FLX). The resulting in-silico indices demonstrated that covering the PR entails less thrombogenic patterns than uncovering it. In our study, disk-based devices had better adaptability to complex LAA morphologies and a slightly minor associated risk of DRT than non-disk devices.

Keywords: atrial appendage · occluder device · thrombus · particle model · fluid dynamic

1 Introduction

The risk of thrombus formation in the left atrial appendage (LAA) is increased in patients with atrial fibrillation (AF). When oral anticoagulants (OAC) are contraindicated to AF patients, left atrial appendage occlusion (LAAO) stands as a suitable alternative. Nevertheless, some complications are associated to LAAO interventions, including peri-device bleeding, device migration and device-related thrombus (DRT). Regarding DRT, a large variability on its prevalence has been reported, ranging from 1% to 7% of the patients [1]. According to these studies,

DRT seems to be ruled by multiple factors, such as an incomplete endothelialization of the device and the presence of thrombogenic patterns (i.e., low velocity re-circulations and vortex structures, high wall shear stress). For instance, recent investigations [1, 2] have demonstrated that in most patients developing DRT, the thrombus was formed in the PR region, with the LAAO not covering it. Additionally, low velocities ($\leq$ 0.2 m/s) near the LAA have been associated with an increased risk of DRT [3].

In LAAO planning, it is crucial to accurately explore and understand the LA/LAA geometry of the patient since it is highly variable and fully determine which device, and where, is going to be implanted. To characterize LAA morphology, the most used imaging techniques are transesophageal echocardiography (TEE) and X-ray, but Computed Tomography (CT) is starting to have a relevant role for this purpose as well [4]. Unfortunately, standard imaging techniques provide limited information about LA and LAA haemodynamics, which is critical for DRT analysis. Several in-silico models with fluid simulations in the LA are available in the literature (e.g., [5–7] as some recent ones), including thrombus models with Discrete Phase Modelling (DPM) approaches [8], which contribute to better understand blood flow patterns in the LA under different conditions. Some investigators [9–11] have also incorporated LAAO devices to study the influence of device settings on post-procedure haemodynamic outcomes such as DRT, but only in a limited number of LAAO options and LA geometries, without considering thrombus models. The main objective of this study was the evaluation of DRT after LAAO through the in-silico analysis of simulated blood flow patterns and platelet deposition (with DPM) with different LAAO types (Amplatzer Amulet from Abbott Vascular, Santa Clara, CA, USA; and Watchman FLX from Boston Scientific, Malborough, Massachusetts, USA) and positions (covering or not the PR) on six different patient-specific LA/LAA geometries extracted from CT images.

2 Materials and Methods

2.1 Data acquisition and modelling pipeline

The LA geometries of the six cases that were assessed in this work were obtained from the segmentation of CT images of patients from Hôpital Cardiologique du Haut-Lévêque (Bordeaux, France). Three-dimensional cardiac CT studies were performed on a 64-slice dual Source CT system (Siemens Definition, Siemens Medical Systems, Forchheim, Germany). CT scans were reconstructed into isotropic voxel sizes (ranged between 0.37-0.5 mm; 512 x 512 x [270-403] slices). The Hôpital Cardiologique du Haut-Lévêque ethical committees approved this study and patients had given written informed consent.

Different scenarios were tested using the modelling pipeline shown in Figure 1. First, the LA was segmented from pre-procedural CT images using region-growing and thresholding tools available in 3D Slicer[3]. The surface meshes including the deployed device (built using Computational Aided Design software)

[3] https://www.slicer.org/

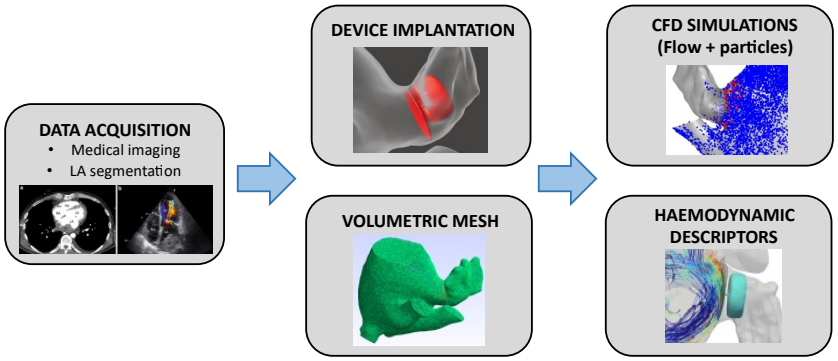

Fig. 1. Modelling pipeline, based on Computational Fluid Dynamics (CFD) simulations, for the in-silico analysis of device-related thrombus after left atrial appendage occlusion (LAAO).

in the LAA were built using Meshmixer[4]. Some simplifications needed to be made to achieve high-quality meshes (e.g., removal of anchors in Amulet device). During implantation, we considered rigid walls for the LA surface and a deformable device. Then, volumetric meshes were generated and, after conducting the CFD simulations, the resulting flow field and associated risk of DRT were assessed using different techniques of flow visualization and quantification.

For each LA geometry, the two studied positions (covering and uncovering the PR) were previously defined and assessed before implanting the device, with the help of interventional cardiologists from the Hôpital de Haut-Lévêque (Bordeaux). The size of the implanted device in each case was assessed using the VIDAA platform [9], based on morphological measurements such as the LAA ostium size and LAA depth. A total of 24 different configurations were successfully completed after placing the deployed devices at the corresponding positions in all studied geometries.

2.2 Haemodynamic simulations

Blood flow was simulated using Ansys Fluent 19.2 (Ansys, Inc. Pennsylvania, USA[5]). Blood was considered as an incompressible Newtonian fluid in a laminar regime, with a density and viscosity of $\rho = 1060$ kg/m^3 and $\mu = 0.0035$ kg/m·s. Three cardiac beats were simulated. In all cases the same boundary conditions were assumed: pressure inlet boundary conditions were set in all pulmonary veins (PV) with a profile extracted from an AF patient (in sinus rhythm); velocity outlet boundary conditions were set in the mitral valve (MV) from Doppler data from each studied patient. A spring-based dynamic mesh model was applied to include LA wall movement, considering the MV ring plane as a moving boundary as defined in [12]. Out of the resulting CFD simulations, blood flow velocities and

[4] meshmixer.com
[5] https://www.ansys.com/products/fluids/ansys-fluent

Table 1. Mean velocities during the second cardiac cycle in a region near the device, in systole (Sys) and diastole (Dias). In bold, values below 0.2 m/s. PR: pulmonary ridge.

Average velocities near the device (m/s)								
	PR covered				PR uncovered			
	Amulet		Watchman		Amulet		Watchman	
	Sys	Dias	Sys	Dias	Sys	Dias	Sys.	Dias
Case 1	**0.11**	0.29	**0.12**	0.30	**0.10**	**0.17**	**0.13**	**0.19**
Case 2	**0.16**	0.28	**0.18**	0.29	**0.11**	**0.18**	**0.07**	**0.17**
Case 3	**0.16**	0.39	**0.17**	0.37	**0.14**	0.34	**0.16**	0.29
Case 4	**0.19**	0.36	**0.18**	0.36	**0.11**	0.22	**0.11**	0.25
Case 5	**0.09**	**0.13**	**0.07**	**0.12**	**0.05**	**0.08**	**0.02**	**0.05**
Case 6	0.22	0.29	**0.18**	0.25	**0.09**	**0.16**	**0.13**	**0.15**

several in-silico indices were estimated to assess the risk of DRT. For instance, as in previous works [11], we estimated the endothelial cell activation potential (ECAP) index, which is the ratio between the time average wall shear stress (TAWSS) and oscillatory shear index (OSI), since it points to regions with low velocities and complex flows, thus prone to DRT. Additionally, the Lambda-2 and Q-criterion were computed to visually identify regions with vortices in blood flow patterns. Both metrics depend of the rotational (i.e., vorticity) and strain rate tensors. For this study, a Lambda-2 with negative value (-50) was used for vortex identification, as in other studies focused in the human heart [13].

2.3 Platelet adhesion model

A discrete phase was added to the continuous phase (blood flow) in the simulations to assess the platelet attachment to the LAA and better evaluate DRT risk. During simulations, particles were injected through the PV inlet, which were then dragged by the flow until they got attached to the LAA or escaped though the MV. Particles were assumed to be clusters of platelets, thus the values of density ρ_p, viscosity μ_p, surface tension σ_p and platelet concentration in blood c_p were taken accordingly. Particle trajectories were computed individually by integrating the force balance of each particle within the continuous phase, which reads:

$$m_p \frac{d\mathbf{u}_p}{dt} = m_p \frac{\mathbf{u} - \mathbf{u}_p}{\tau_r} + \mathbf{F}, \tag{1}$$

where m_p is the particle mass, $\mathbf{u}$ the fluid phase velocity, $\mathbf{u}_p$ the particle velocity and ρ the fluid density. The term $m_p\left(\mathbf{u} - \mathbf{u}_p\right)/\tau_r$ corresponds to the drag force, where τ_r is the droplet relaxation time. An extra term, $\mathbf{F}$, with the Saffman lift force was included due to the influence of shear rate in the particle attachment process.

Particles were injected through the PV surfaces during the first 10 time steps at the beginning of each beat. We assumed that, in the first injection, the number of injected particles, n_{part}, corresponded to a platelet concentration in blood of

$c_p = 2 \cdot 10^8$ mL^{-1}, which is within the normal range in physiological conditions[6]. In order to fulfill this requirement, the following parameters were computed: the number of platelets per cluster, n_{ppc}; the particle diameter, d_p; and the total flow rate, Q. For the platelet models, the following values were assumed: number of time steps during the injection $n_{ts} = 10$, diameter of platelets $d_{plat} = 3$ μm, particle density $\rho_p = 1550$ kg m^{-3} and time steps for the injection $\Delta t = 0.01$ s. As we fixed concentration, all these parameters were dependent on the LA volume (V_{LA}). Therefore, the number of platelets per injection n_{plat}, was computed as: $n_{plat} = c_p \cdot V_{LA}$. In order to assess DRT, the number of particles attached to the LAA and their location were analyzed at the end of the simulations. To do so, the LAA surface was separated from the rest of the LA and a wall-film condition was assumed. This condition implied that any particle that touched the LAA, independently of its velocity, was stuck to the surface; they could eventually be detached from the LAA if the flow would drag them to the LAA boundary.

3 Results and discussion

Table 1 displays the mean velocities obtained from fluid simulations for all studied cases and LAAO configurations. Mean velocities were below 0.2 m/s in almost all cases during systole, with the exception of Case 6 in the covered PR position with Amulet device. Low velocities during diastole were less common, due to the proximity of the LAA to the MV, which is open during this phase. Additionally, a higher incidence of low velocities in uncovered PR configurations was encountered, thus a higher risk of DRT. On the other hand, no significant differences between the two devices (i.e., Amulet and Watchman FLX) were encountered in this regard.

Figure 2 shows the four analyzed LAAO configurations (i.e., pulmonary ridge covered/uncovered and Amulet/Watchman FLX devices) for one LA geometry (Case 5), in the form of blood flow streamlines colored by the velocity magnitude and vorticity indices. As a general rule, flow re-circulation patterns with low velocities (i.e., conditions required for DRT) were commonly detected at the edge of Watchman FLX at some point during the cardiac cycle, independently of the position of the occluder. Same conclusions were drawn from the analysis of vorticity indices. Conversely, vortices with low velocities were rarely detected in the covered PR configurations with the Amulet device. However, vortices were present in the uncovered PR position both for Amulet and Watchman FLX devices, being slightly more common in systole than in diastole. The Watchman FLX device was also related with higher ECAP values (i.e., more risk of DRT) in the neighborhood of the device than the Amulet device. As a general rule no relevant differences were appreciated between the ECAP maps of the covered and uncovered PR positions.

Figure 3 shows the platelet distribution at end diastole of the second cardiac cycle for some of the studied cases. It can be observed that platelets did not only stack in the PR region, but they got attached to other uncovered regions of the

[6] https://bionumbers.hms.harvard.edu/search.aspx

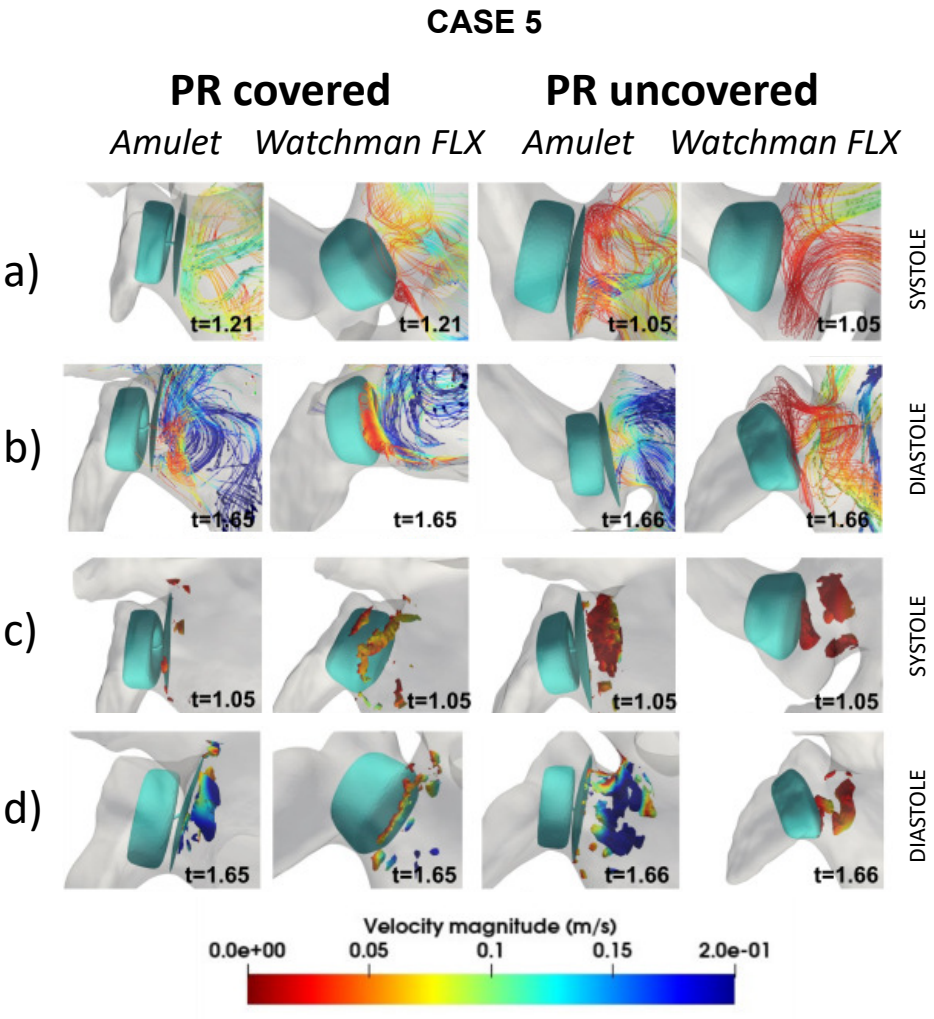

Fig. 2. Results for covered/uncovered pulmonary ridge (PR) for one of the studied geometries (Case 5). a)b) Blood flow streamlines colored by velocity magnitude (systole and diastole, respectively). c)d) Vorticity index, with isovolumes defined by $\lambda_2 = -50$ (systole and diastole, respectively). Time is expressed in seconds.

LAA. However, for the uncovered position for geometries 2 and 6, a significant amount of platelets clustered in the PR region rather than in other zones, in agreement with literature [2]. Overall, 75% of the analyzed configurations has more platelets attached to the LAA (i.e., more risk of DRT) with an uncovered PR, as can be seen in Figure 4a (yellow and purple bars higher than blue and red ones in all cases). Also, the Watchman FLX device appeared to have more platelets prone to get attached to the LAA than the Amulet one.

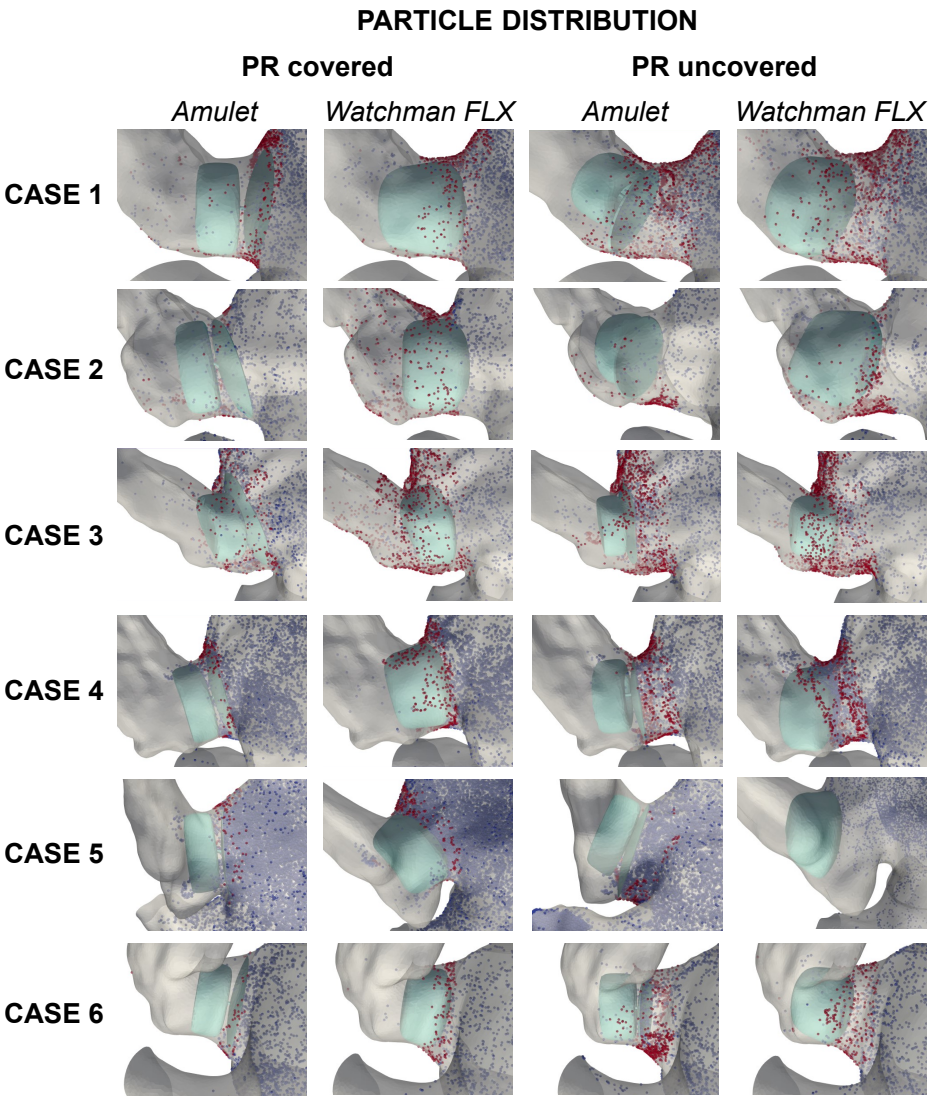

Fig. 3. Particle distribution in the left atrial appendage in diastole for the two analyzed devices (Amulet and Watchman FLX) in the covered and uncovered pulmonary ridge (PR) configuration. A higher density of attached particles (red) would be associated to a higher risk of device-related thrombus. Blue: free particles.

4 Conclusions

A modelling pipeline has been developed to predict the risk of DRT after the implantation of different LAAO devices in several positions within six LA/LAA morphologies. According to the resulting haemodynamic in-silico indices, un-

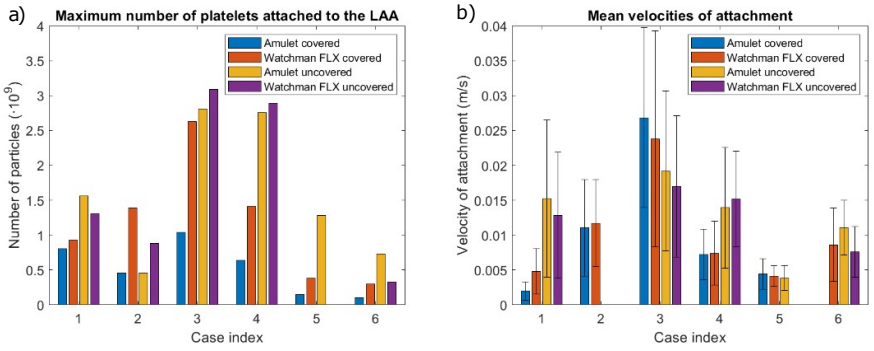

Fig. 4. *a) Maximum number of platelets attached to the left atrial appendage (LAA). b) Mean velocity of attachment for all the studied configurations (Cases 1-6): Amulet-uncovered pulmonary ridge (PR) (blue); Watchman FLX-uncovered PR (orange); Amulet - covered PR (yellow); and Watchman FLX - covered PR (purple).*

covered PR device configurations generated more thrombogenic patterns, which was confirmed by the DPM analysis. Moreover, the Amplatzer Amulet device showed less cases with low-velocity swirls and vortices than the Watchman FLX, thus being less prone to DRT after implantation, arguably due to the presence of the disk in the device design. Future work will mainly focus on establishing a robust and rigorous validation framework for the fluid simulations, using advanced imaging such as 4D flow magnetic resonance imaging and blood speckle tracking as well as in-vitro set-ups like the one recently proposed by Dueñas-Pamplona et al. [14].

Acknowledgments This work was supported by the Agency for Management of University and Research Grants of the Generalitat de Catalunya under the the Grants for the Contracting of New Research Staff Programme - FI (2020 FI_B 00608) and the Spanish Ministry of Economy and Competitiveness under the Programme for the Formation of Doctors (PRE2018-084062), the Maria de Maeztu Units of Excellence Programme (MDM-2015-0502) and the Retos Investigación project (RTI2018-101193-B-I00). Additionally, this work was supported by the H2020 EU SimCardioTest project (Digital transformation in Health and Care SC1-DTH-06-2020; grant agreement No. 101016496).

References

1. Adel Aminian, Boris Schmidt, and Patrizio Mazzone et al. Incidence, Characterization, and Clinical Impact of Device-Related Thrombus Following Left Atrial Appendage Occlusion in the Prospective Global AMPLATZER Amulet Observational Study. *JACC: Cardiovascular Interventions*, 12(11):1003–1014, 6 2019.
2. Xavier Freixa, Pedro Cepas-Guillen, and Eduardo Flores-Umanzor et al. Pulmonary ridge coverage and device-related thrombosis after left atrial appendage occlusion. *EuroIntervention*, 16(15):E1288–E1294, 2021.

3. Harutoshi Tamura, Tetsu Watanabe, and Osamu Hirono et al. Low Wall Velocity of Left Atrial Appendage Measured by Trans-Thoracic Echocardiography Predicts Thrombus Formation Caused by Atrial Appendage Dysfunction. *Journal of the American Society of Echocardiography*, 23(5), 2010.
4. Danny H.F. Chow, Gintautas Bieliauskas, and Fadi J. Sawaya et al. A comparative study of different imaging modalities for successful percutaneous left atrial appendage closure. *Open Heart*, 4(2):e000627–e000627, 6 2017.
5. Guadalupe García-Isla, Andy L. Olivares, and Etelvino . Silva et al. Sensitivity analysis of geometrical parameters to study haemodynamics and thrombus formation in the left atrial appendage. *International Journal for Numerical Methods in Biomedical Engineering*, 34(8):1–14, 2018.
6. Alessandro Masci, Martino Alessandrini, and Davide Forti et al. A Proof of concept for computational fluid dynamic analysis of the left atrium in atrial fibrillation on a patient-specific basis. *Journal of Biomechanical Engineering*, 142(1), jan 2020.
7. Manuel García-Villalba, Lorenzo Rossini, and Alejandro Gonzalo et al. Demonstration of patient-specific simulations to assess left atrial appendage thrombogenesis risk. *Frontiers in physiology*, 12:596596–596596, 02 2021.
8. Yan Wang, Yonghui Qiao, Yankai Mao, Chenyang Jiang, Jianren Fan, and Kun Luo. Numerical prediction of thrombosis risk in left atrium under atrial fibrillation. *Mathematical Biosciences and Engineering*, 17(3):2348–2360, 2 2020.
9. Ainhoa M. Aguado, Andy L. Olivares, Carlos Yagüe, Etelvino Silva, Marta Nuñez-García, and Álvaro Fernandez-Quilez et al. In silico Optimization of Left Atrial Appendage Occluder Implantation Using Interactive and Modeling Tools. *Frontiers in Physiology*, 10(MAR):237, 3 2019.
10. Jordi Mill, Andy L. Olivares, Dabit Arzamendi, Victor Agudelo, Ander Regueiro, Oscar Camara, and Xavier Freixa. Impact of Flow Dynamics on Device-Related Thrombosis After Left Atrial Appendage Occlusion. *Canadian Journal of Cardiology*, 36(6):13–968, 6 2020.
11. Jordi Mill, Victor Agudelo, Chi et al. Hion Li et al., Jerome Noailly, Xavier Freixa, Oscar Camara, , and Dabit Arzamendi. Patient-specific flow simulation analysis to predict device-related thrombosis in left atrial appendage occluders. *REC: interventional cardiology (English Edition)*, jul 2021.
12. Federico Veronesi, Cristiana Corsi, and Lissa Sugeng et al. Quantification of Mitral Apparatus Dynamics in Functional and Ischemic Mitral Regurgitation Using Real-time 3-Dimensional Echocardiography. *Journal of the American Society of Echocardiography*, 21(4):347–354, 4 2008.
13. Mohammed S.M. El Baz, Boudewijn P.F. Lelieveldt, Jos J.M. Westenberg, and Rob J. Van Der Geest. Automatic extraction of the 3D left ventricular diastolic transmitral vortex ring from 3D whole-heart Phase Contrast MRI using Laplace-Beltrami signatures. In *Lecture Notes in Computer Science (including subseries Lecture Notes in Artificial Intelligence and Lecture Notes in Bioinformatics)*, volume 8330 LNCS, 2014.
14. Jorge Dueñas-Pamplona, José Sierra-Pallares, Javier García, Francisco Castro, and Jorge Munoz-Paniagua. Boundary-Condition Analysis of an Idealized Left Atrium Model. *Annals of Biomedical Engineering*, 49(6):1507–1520, jan 2021.